THE JOURNAL OF NAVIGATION (2019), 1–18.
doi:0000000000

An Intelligent Quaternion SVDCKF AHRS Estimation with Variable Adaptive Methods in Complex Conditions

Yue Yang, Xiaoxiong Liu, Weiguo Zhang, Xuhang Liu and Yicong Guo

(School of Automation, Northwestern Polytechnical University,China)
(E-mail: liuxiaoxiong@nwpu.edu.cn)

Aimed at solving the problem of Attitude and Heading Reference System(AHRS) in the complex and dynamic conditions for small-UAV, An intelligent Singular Value Decomposition Cubature Kalman Filter(SVDCKF) combined with the Variable Adaptive Methods(VAM) is proposed in this paper. Considering the nonlinearity of quaternion AHRS model and non-positive definite of the state covariance matrix, the SVDCKF algorithm is presented with both the SVD and CKF in order to better obtain the filter accuracy and reliability. Additionally, there are the different changes of the values in the accelerometer measurement resulting from the complex flying conditions. Thus, the VAM is designed to deal with three-axis values of the acceleration and tune intelligently the measurement noise matrix R_a. Moreover, the heading measurement from the three-axis values of the magnetometer is calculated according to the whether to use the three-axis values of the acceleration in the special situations. The simulation and experiment results demonstrate that the proposed filter algorithm has the more excellent attitude solution accuracy and robustness than both the Complementary Filter(CF) and the Error State Kalman Filter(ESKF).

KEYWORDS

AHRS. small-UAV. SVDCKF. Variable Adaptive Methods. nonlinearity.

1. INTRODUCTION. Unmanned aerial vehicle(UAV) has been become increasingly important role in more and more applications, e.g. in the aerial surveillance(McNeal, 2014), three-dimensional mapping model(Verhoeven, 2011) and search rescue(Karaca et al., 2018) so on. The attitude and heading reference system is the key parts of the autonomous unmanned flight systems(AUFS), and the AHRS is composed of the gyroscope, accelerometer, magnetometer and the microprocessor, and using the information fusion algorithm to calculate the attitude without the assistance of other sensors data. The main focus of this paper is the study of the accurate and reliable AHRS algorithm for the small-UAV.

In recent years, the current research on the AHRS algorithm mainly includes the CF, gradient descent filter and nonlinear Kalman Filter so on. The CF utilizes mutual compensation characteristics of the signal frequency from the multiple sensors, solving the sensor noises

in the frequency domain, and fusing the different sensor measurement values to calculate the attitude. A nonlinear CF AHRS algorithm is proposed by the Mahony(Euston et al., 2008, September), which combines the low-cost IMU and magnetometer through a first-order dynamic model to provide the reliable attitude estimation parameters. Jin Wu(Wu et al., 2016) proposed a fast CF fusion algorithm based on the quaternion attitude estimation, and designed the step-by-step filtering to eliminate the influence of outliers of the magnetometer, it is highly efficient in terms of solution accuracy in real-time performance. Moreover, in order to tune the sensor noises, Qingquan Yang(Yang et al., 2018) proposed a fast adaptive gain CF algorithm for attitude estimation in high dynamic operating conditions, and achieving a good performance in accuracy. In addition to the CF, the gradient descent filter is often used in AHRS estimation, and to be an iterative algorithm for finding the optimal values. The specific implementation process is to search the solution according to the negative direction of the slope in the objective function. Madgwick(Madgwick et al., 2011, June) used the gradient descent method for AHRS calculation, which is intended to be used in human motion tracking system. It used quaternion to update attitude, and used the accelerometer and magnetometer to calculate the gyroscope measurement error as the quaternion derivative for being optimal gradient descent ayalysis.

The Kalman Filter(Welch et al., 1995; Meinhold et al., 1983; Burgers et al., 1998) is the optimal estimation algorithm that fuses the multiple sensors data with noises in the actual environment, and often used as an optimal estimator in the Gaussian distribution noise systems. However, the Kalman Filter is generally used in the linear systems. The AHRS model has nonlinearity in the practical applications. Thus, the nonlinear Kalman Filter(Wang et al., 2012) has been widely studied by the scholars around the world. Aimed at the AHRS of UAV, Song Yu(Song et al., 2015) proposed a quaternion EKF algorithm and designed adaptive filter to correct the measurement noise covariance matrix, which not only solved the problem of large errors about MEMS devices, but also reduced the influence of random errors for the gyroscope on attitude estimation. Yong Liang(YongLiang et al., 2008, September) proposed an improved EKF algorithm to estimate the small helicopters attitude, and taking the bidirectional vector systems as the measurement updating, using the flight sensor data to evaluate the filter algorithm performance. Nevertheless, the EKF is the way of first-order Taylor expansion of the function for the nonlinear model, which exists the rounding errors resulting in the problem of divergence and poor filter accuracy. Subsequently, there are some improved nonlinear kalman fiter methods(ZHAO et al., 2009) which include UKF(Wan et al., 2000, October), CKF(Arasaratnam et al., 2009) and PF(Arulampalam et al., 2002) so on. Pourtakdoust(Pourtakdoust et al., 2007) proposed the quaternion orientation estimation based on the adaptive Unsecnted Kalman Filter, which can capture the effect of nonlinear AHRS model up to second-order without the need for explicit calculations of the Jacobians matrixs. The CKF uses the cubature sample points to approximate the nonlinear model that can up to the third-order compared to the UKF. Although, the PF is a sequential important sampling filter method based on the bayesian sampling estimation, which has better filter accuracy compared with both UKF and CKF. However, there are some disadvantages of the large calculation quantity and the poor real-time. Additionally, the PF is prone to occur the problem of particle starvation causing the filter divergence.

In acutally, when the nonlinear AHRS system is in the operating environment, it is affected by the uncertain factor of the measurement sensors noise that its statistical characteristics are changed in complex conditions. An adaptive version of the filter is proposed

by Choukroun(Choukroun et al., 2006) to handle modelling errors of the dynamic system noise statistics, which are presented a Novel Kalman Filter for estimating the attitude. In order to improve the performance of real-time and sensors noise covariance, a simplified and novel adaptive Kalman Filter algorithm(Zhang et al., 2015) are designed for the attitude estimation of the multi-rotor UAV, can solve the problem of the noise statistical characteristics. However, there are different sensors noise statistical characteristics in the complex environments, the Wang(Wang et al., 2004) and Li(Li et al., 2013) all designed the adaptive gain methods to tune the measurement noises covariance matrix, it can eliminate the uncertain errors to obtain the reliable attitude calculation.

In this paper, aimed at the characteristics of AHRS model nonlinearity, the CKF combined with the SVD is designed to obtain the better filter accuracy. The decomposition of the QR is substituted by the SVD in order to solve the problem of non-positive definite of the state covariance P. Moreover, for the uncertain sensor noise in different conditions, the VAM for solving the measurement values of the accelerometer and magnetometer is presented to provide the reliable, steady attitude estimation and the good robustness.

The rest of this paper is organized as follows: In Section 2, the mathematical model of the nonlinear AHRS model based on the quaternion solution and the sensor model is introduced; An approach of this study is proposed about SVDCKF fusion algorithm in Section 3; Then, it is designed about the VAM in Section 4; The results of numerical simulation and experimental analysis in Section 5 demonstrate the performance of the proposed algorithm; And conclusion is given in Section 6.

2. MATHEMATICAL MODEL.

2.1. *Quaternion attitude determination.*

The strapdown inertial attitude determination has several expression ways which include euler angles, Direction Cosine Matrix(DCM), quaternion and so on. The euler angles have the phenomenon of "Gimbal Lock" when pitch is 90 degrees, resulting in the failure of attitude solution. There are nine elements and consist of 3 degrees of freedom(DOF) in the DCM, but don't hold on good real-time during the calculation of multiplication and invertible operation. Compared to the previous two methods, the representation of quaternion(Zhang, 1997) is very simple and efficient, and often used to describe the rigid body rotation and attitude transformation.

$$\boldsymbol{Q} = q_0 + q_1\boldsymbol{i} + q_2\boldsymbol{j} + q_3\boldsymbol{k} \tag{1}$$

This paper uses quaternion to update attitude, which is supposed to the moving coordinate system rotating on the fixed axis during the update period. The first-order Runge-Kutta method is used to solve the quaternion differential equation and derived the discrete model in Equation(2).

$$\boldsymbol{Q}(t_k) = \boldsymbol{Q}(t_{k-1}) \otimes \boldsymbol{q}(\Delta t) \tag{2}$$

Where $\boldsymbol{Q}(t_k)$ and $\boldsymbol{Q}(t_{k-1})$ are the normalized quaternion in time of k and k-1, respectively. $\boldsymbol{q}(\Delta t)$ is the quaternion of attitude updating change during the $[t_{k-1}, t_k]$.

$$\boldsymbol{q}(\Delta t) = \exp(\boldsymbol{\Omega}_\omega \Delta t) = \sum_{n=0}^{\infty} \frac{(\boldsymbol{\Omega}_\omega \Delta t)^n}{n!} \simeq (\boldsymbol{I}_{4\times 4} + \frac{\boldsymbol{\Omega}_\omega \Delta t}{2}) \tag{3}$$

Where $\mathbf{\Omega}_\omega$ is the skew-symmetric matrix of the angular velocity about the body coordinate system relative to the navigation coordinate system on the UAV in Equation(4).

$$\mathbf{\Omega}_\omega = \begin{bmatrix} 0 & -\omega_x & -\omega_y & -\omega_z \\ \omega_x & 0 & \omega_z & -\omega_y \\ \omega_y & -\omega_z & 0 & \omega_x \\ \omega_z & \omega_y & -\omega_x & 0 \end{bmatrix} \tag{4}$$

Where $\boldsymbol{\omega}$ is three-axis angular velocity for gyroscope in the body coordinate system, which is ignored the effect of cone error and earth rotation angular rate for the low-cost MEMS and the application of near-ground navigation.

$$\begin{cases} \phi = atan2(2(q_0q_1 + q_2q_3), 1 - 2(q_1^2 + q_2^2)) \\ \theta = asin(2(q_0q_2 - q_1q_3)) \\ \psi = atan2(2(q_0q_3 - q_1q_2), 1 - 2(q_1^2 + q_2^3)) \end{cases} \tag{5}$$

Where ϕ, θ and ψ are the roll, ptich and yaw of the UAV, respectively. Moreover, the range of ϕ and ψ are $[-\pi, \pi]$, and θ is $[-\frac{\pi}{2}, \frac{\pi}{2}]$ in the Equation(5).

2.2. *Sensor model.* The low-cost sensors of AHRS, which includes gyroscope, accelerometer and magnetometer, are fixed to the body of the UAV. Moreover, the measurement coordinate axis of the sensors are orthogonal each other and consistent with the body coordinate system in the ideal conditions. The sensor model is listed in Equation(6).

$$\begin{cases} \hat{\boldsymbol{\omega}}(t) = k_\omega \boldsymbol{\omega}(t) + \boldsymbol{b}_\omega(t) + \boldsymbol{n}_\omega(t) \\ \hat{\boldsymbol{a}}(t) = k_a(\boldsymbol{a}(t) + \boldsymbol{C}_n^b \boldsymbol{g}) + \boldsymbol{b}_a(t) + \boldsymbol{n}_a(t) \\ \hat{\boldsymbol{m}}(t) = k_m \boldsymbol{m}(t) + \boldsymbol{b}_m(t) + \boldsymbol{n}_m(t) \end{cases} \tag{6}$$

Where $\hat{\boldsymbol{\omega}}(t)$, $\hat{\boldsymbol{a}}(t)$ and $\hat{\boldsymbol{m}}(t)$ are the measurement of angular velocity, acceleration and magnetic field strength, respectively. This paper assumes that the sensors have been calibrated before being used, which means that the scale factors(k_ω, k_a, k_m) are 1. The terms of $\boldsymbol{b}_\omega(t)$, $\boldsymbol{b}_a(t)$ and $\boldsymbol{b}_m(t)$ represent the measurement bias that vary slowly over time, which can be estimated as the part of the filter states. The additive noise terms($\boldsymbol{n}_\omega(t)$, $\boldsymbol{n}_a(t)$, $\boldsymbol{n}_m(t)$) that fluctuate rapidly assumed to be the Gaussian white noise with power spectral density.

The common way of identifying the IMU noise is Allan variance analysis(Allan, 1966) used in this paper. In addition, the measurement of local magnetic field disturbed with magnetic distortion can be removed by calibrating the magnetometer(Allotta et al., 2016; Roetenberg et al., 2005)in the unknown environment.

2.3. *Stochastic system model.* The AHRS estimation that we meet is usually the nonlinear system in the actual situations, thus the dynamic and observation discrete equations of stochastic system model are established under the nonlinear Gaussian conditions.

$$\begin{cases} x_k = f(x_{k-1}, v_{k-1}) + m_{k-1} \\ z_k = h(x_k) + n_k \end{cases} \tag{7}$$

Where x_k is state estimation parameters, $f(.)$ is the nonlinear dynamic function, v_k is the system input, m_k is the process noises which are assumed the zero-mean Gaussian white

noise. z_k is the observation parameters, $h(.)$ is the nonlinear measurement function, n_k is the observation noises which are also assumed the zero-mean Gaussian white noise.

$$\begin{cases} E[m_k] = 0 & E[m_k m_j^T] = Q_k \delta_{k,j} \\ E[n_k] = 0 & E[n_k n_j^T] = R_k \delta_{k,j} \\ E[m_k n_j^T] = 0 & E[x_0 m_k^T] = 0 \qquad E[x_0 n_k^T] = 0 \end{cases} \tag{8}$$

Where Q_k is the process noise covariance, R_k is the observation noise covariance, and $\delta_{k,j}$ is Kronecker delta function.

2.4. *Nonlinear AHRS model.* It is necessary that designs the good AHRS model for attitude solution. Thus, it is given that the nonlinear AHRS model in Equations(9)(10)(11) after discussing and analyzing the attitude determination and sensor model.

The proposed algorithm has the estimated states which are the attitude quaternions $\boldsymbol{Q}(t_k) = [q_0(t_k), q_1(t_k), q_2(t_k), q_3(t_k)]$, three-axis gyro bias $\boldsymbol{b}_\omega(t_k)$ and three-axis accel bias $\boldsymbol{b}_a(t_k)$ in the body coordinate system. The dynamic model of AHRS is derived in Equation(9).

$$\boldsymbol{x}(t_k) = \begin{bmatrix} \boldsymbol{Q}(t_k) \\ \boldsymbol{b}_\omega(t_k) \\ \boldsymbol{b}_a(t_k) \end{bmatrix} = \begin{bmatrix} (\boldsymbol{I}_{4\times4} + \frac{\boldsymbol{\Omega}_\omega \Delta t}{2}) \boldsymbol{Q}(t_{k-1}) \\ \boldsymbol{b}_\omega(t_{k-1}) \\ \boldsymbol{b}_a(t_{k-1}) \end{bmatrix} + \begin{bmatrix} \boldsymbol{m}_Q(t_{k-1}) \\ \boldsymbol{m}_\omega(t_{k-1}) \\ \boldsymbol{m}_a(t_{k-1}) \end{bmatrix} \tag{9}$$

Where $\boldsymbol{m}_Q(t_{k-1})$, $\boldsymbol{m}_\omega(t_{k-1})$ and $\boldsymbol{m}_a(t_{k-1})$ are the corresponding process noise with Gaussian for the corresponding states, namely $\boldsymbol{m}_Q(t_{k-1}) \sim \mathcal{N}(0, \sigma_Q^2)$, $\boldsymbol{m}_\omega(t_{k-1}) \sim \mathcal{N}(0, \sigma_\omega^2)$ and $\boldsymbol{m}_a(t_{k-1}) \sim \mathcal{N}(0, \sigma_a^2)$.

For the problem of inconsistent sensors updating frequency in observation model, it can be considered that list the equations of each sensor seperately. The measurement of the specific acceleration, written in the form of the $[a_x(t_k), a_y(t_k), a_z(t_k)]$, delivered by accelerometer, and can be designed in Equation(10).

$$\boldsymbol{z}_a(t_k) = \begin{bmatrix} a_x(t_k) \\ a_y(t_k) \\ a_z(t_k) \end{bmatrix} = \begin{bmatrix} -2g(q_1(t_k)q_3(t_k) - q_0(t_k)q_2(t_k)) \\ -2g(q_2(t_k)q_3(t_k) + q_0(t_k)q_1(t_k)) \\ -g(q_0^2(t_k) - q_1^2(t_k) - q_2^2(t_k) + q_3^2(t_k)) \end{bmatrix} + \boldsymbol{n}_a(t_k) \tag{10}$$

Where g is the local gravity acceleration about 9.80665 m/s^2, and $\boldsymbol{n}_a(t_k) \sim \mathcal{N}(0, R_a^2)$ is the measurement noise of accelerometer. However, the acceleration value is greatly affected by linear acceleration and uncertain vibration, it can occur the large errors in attitude of UAV used accelerometer alone, especially in large maneuvers. This paper solves this situation in the later section.

During the correcting the yaw, the measurements of magnetometer obtained the local magnetic field strength can be described in Equation(11).

$$\begin{aligned} z_m(t_k) = \psi_m(t_k) = atan2(&-2(q_1(t_k)q_2(t_k) - q_0(t_k)q_3(t_k)), \\ &(q_0^2(t_k) - q_1^2(t_k) + q_2^2(t_k) - q_3^2(t_k))) \\ &+ n_m(t_k) \end{aligned} \tag{11}$$

Where the $\psi_m(t_k)$ is the heading observation angle calculated by projecting the value of magnetometer on the horizontal plane. Actually, there are different ways of calculating the

heading observation angle when the UAV is in the different flying conditions, and be dealt with this problem in the later section.

3. SVD-CKF. The CKF(Arasaratnam et al., 2009; Cui et al., 2018) can provide a systematic solution for high-dimensional nonlinear filtering problem that also includes the nonlinear AHRS calculation, it has at least the third-order Taylor series approximation for nonlinear functions compared with the EKF and UKF in the solution accuracy, and it uses the Cholesky decomposition of state covariance matrix $\boldsymbol{P}$, $\boldsymbol{P} = \boldsymbol{U}^T\boldsymbol{U}$, and $\boldsymbol{U}$ is the triangular matrix. Nevertheless, it can be found several disadvantages during using the Cholesky decomposition:

1) The Cholesky decomposition defines the matrix $\boldsymbol{P}$ accorded with the properties of the positive definite or symmetric positive definite, and limits the range of the initial value of $\boldsymbol{P}$.

2) The matrix $\boldsymbol{P}$ can become the sparse matrix during the running period of filter algorithm, and destroys the requirements of the Cholesky decomposition.

This paper employs the Singular Value Decomposition(SVD)(Zhang et al., 2015) to replace the Cholesky decomposition for handling the matrix $\boldsymbol{P}$ which can be expanded to the arbitrary matrix.

$$\boldsymbol{P} = \boldsymbol{U}\boldsymbol{S}\boldsymbol{V}^T \tag{12}$$

Where $\boldsymbol{P}$ is the dimensions of $m \times m$ arbitrary matrix, $\boldsymbol{U}$ and $\boldsymbol{V}$ are the unit orthogonal matrix, respectively. the $\boldsymbol{S}$ is the diagonal matrix that has the elements called the "singular valuer", and $\boldsymbol{U} \in R^{m\times m}$, $\boldsymbol{S} \in R^{m\times n}$ and $\boldsymbol{V} \in R^{n\times n}$, respectively.

$$\boldsymbol{S} = \begin{bmatrix} s_1 & 0 & 0 & 0 & 0 \\ 0 & s_2 & 0 & 0 & 0 \\ 0 & 0 & s_3 & 0 & 0 \\ 0 & 0 & 0 & \ddots & 0 \\ 0 & 0 & 0 & 0 & s_n \end{bmatrix} \tag{13}$$

Thus, this paper summarizes the SVDCKF algorithm writing the explicit steps as follows:

step 1 The setting of initial value $\hat{\boldsymbol{x}}_{0|0}$ and $\hat{\boldsymbol{P}}_{0|0}$ in the filter algorithm and calculating the cubature points ξ_i and weight ω_i based on the multi-dimension spherical-radial rule.

$$\begin{cases} \hat{\boldsymbol{x}}_{0|0} = E(\boldsymbol{x}_0) \\ \hat{\boldsymbol{P}}_{0|0} = E[(\boldsymbol{x}_0 - \hat{\boldsymbol{x}}_{0|0})(\boldsymbol{x}_0 - \hat{\boldsymbol{x}}_{0|0})^T] \end{cases} \tag{14}$$

Where$E(.)$ is the expectation.

$$\begin{cases} \xi_i = \sqrt{\dfrac{m}{2}}[\mathbf{1}]_i \\ \omega_i = \dfrac{1}{m}, i = 1, 2, ..., m = 2n \end{cases} \tag{15}$$

Where n is the dimensions of filter state, m is the number of cubature points, and $[\mathbf{1}]_i$ is the same points as the following set of points:

$$\left\{ \begin{pmatrix} 1 \\ 0 \end{pmatrix}, \begin{pmatrix} 0 \\ 1 \end{pmatrix}, \begin{pmatrix} -1 \\ 0 \end{pmatrix}, \begin{pmatrix} 0 \\ -1 \end{pmatrix} \right\}$$

step 2 State prediction(k = 1,2,3,...):

The covariance matrix $\hat{\boldsymbol{P}}_{k-1|k-1}$ is decomposed by the Equation(16).

$$\hat{\boldsymbol{P}}_{k-1|k-1} = \boldsymbol{U}_{k-1|k-1}\boldsymbol{S}_{k-1|k-1}\boldsymbol{V}^T_{k-1|k-1} \tag{16}$$

Where $\hat{\boldsymbol{P}}_{k-1|k-1}$ is the symmetric matrix, and so $\boldsymbol{U}_{k-1|k-1} = \boldsymbol{V}_{k-1|k-1}$.

Evaluate the cubature points$(i = 1, 2, ..., m)$

$$\boldsymbol{X}_{i,k-1|k-1} = \boldsymbol{U}_{i,k-1|k-1}(\sqrt{\boldsymbol{S}_{k-1|k-1}})\xi_i + \hat{\boldsymbol{x}}_{k-1|k-1} \tag{17}$$

Evaluate the propagated cubature points through the nonlinear dynamic function $f(.)(i = 1, 2, ..., m)$

$$\boldsymbol{X}^*_{i,k|k-1} = f(\boldsymbol{X}_{i,k-1|k-1}, u_{k-1}) \tag{18}$$

Estimate the predicted state and error covariance

$$\begin{cases} \hat{\boldsymbol{x}}_{k|k-1} = \dfrac{1}{m}\displaystyle\sum_{i=1}^{m} \boldsymbol{X}^*_{i,k|k-1} \\ \hat{\boldsymbol{P}}_{k|k-1} = \dfrac{1}{m}\displaystyle\sum_{i=1}^{m} \boldsymbol{X}^*_{i,k|k-1}\boldsymbol{X}^{*T}_{i,k|k-1} - \hat{\boldsymbol{x}}_{k|k-1}\hat{\boldsymbol{x}}^T_{k|k-1} + \boldsymbol{Q}_{k-1} \end{cases} \tag{19}$$

step 3 State correction(k = 1,2,3,...):

The covariance matrix $\hat{\boldsymbol{P}}_{k|k-1}$ is decomposed by the Equation(20).

$$\hat{\boldsymbol{P}}_{k|k-1} = \boldsymbol{U}_{k|k-1}\boldsymbol{S}_{k|k-1}\boldsymbol{V}^T_{k|k-1} \tag{20}$$

Evaluate the cubature points$(i = 1, 2, ..., m)$

$$\boldsymbol{X}_{i,k|k-1} = \boldsymbol{U}_{i,k|k-1}(\sqrt{\boldsymbol{S}_{k|k-1}})\xi_i + \hat{\boldsymbol{x}}_{k|k-1} \tag{21}$$

Evaluate the propagated cubature points through the nonlinear observation function $h(.)$ $(i = 1, 2, ..., m)$

$$\boldsymbol{Z}_{i,k|k-1} = h(\boldsymbol{X}_{i,k|k-1}, u_k) \tag{22}$$

Estimate the predicted measurement, the innovation covariance matrix and the cross-covariance matrix

$$\begin{cases} \hat{\boldsymbol{z}}_{k|k-1} = \dfrac{1}{m}\displaystyle\sum_{i=1}^{m} \boldsymbol{Z}^*_{i,k|k-1} \\ \boldsymbol{P}_{zz,k|k-1} = \dfrac{1}{m}\displaystyle\sum_{i=1}^{m} \boldsymbol{Z}_{i,k|k-1}\boldsymbol{Z}^T_{i,k|k-1} - \hat{\boldsymbol{z}}_{k|k-1}\hat{\boldsymbol{z}}^T_{k|k-1} + \boldsymbol{R}_k \\ \boldsymbol{P}_{xz,k|k-1} = \dfrac{1}{m}\displaystyle\sum_{i=1}^{m} \boldsymbol{X}_{i,k|k-1}\boldsymbol{Z}^T_{i,k|k-1} - \hat{\boldsymbol{x}}_{k|k-1}\hat{\boldsymbol{z}}^T_{k|k-1} \end{cases} \tag{23}$$

Estimate the Kalman filter gain

$$\boldsymbol{K}_k = \boldsymbol{P}_{xz,k|k-1}\boldsymbol{P}^{-1}_{zz,k|k-1} \tag{24}$$

Estimate the updated state and error covariance

$$\begin{cases} \hat{\boldsymbol{x}}_{k|k-1} = \hat{\boldsymbol{x}}_{k|k-1} + \boldsymbol{K}_k(\boldsymbol{z}_k - \hat{\boldsymbol{z}}_{k|k-1}) \\ \hat{\boldsymbol{P}}_{k|k} = \hat{\boldsymbol{P}}_{k|k-1} - \boldsymbol{K}_k\boldsymbol{P}_{zz,k|k-1}\boldsymbol{K}_k^T \end{cases} \tag{25}$$

4. THE VARIABLE ADAPTIVE METHODS.

4.1. *Adaptive solution for acceleration in the different conditions.* The three-axis acceleration values of accelerometer have greatly changed under the different UAV flight conditions, especially some harmful acceleration or outliers can result in the serious impact on the attitude solution. In addition, the body shake and airflow disturbance also occur the uncertainty during flying period. Thus, with the help of adaptive filter(Wang et al., 2004; Li et al., 2013), this paper has proposed the variable dynamic adaptive methods for the different flying environment, which are the stationary condition, low-dynamic condition and high-dynamic condition so on.

This paper defines the dynamic acceleration scalar α in Equation(26).

$$\alpha = |\sqrt{a_{fx}^2 + a_{fy}^2 + a_{fz}^2} - g| \tag{26}$$

Where $[a_{fx}^2, a_{fy}^2, a_{fz}^2]^T$ is the three-axis acceleration values in the body coordinate system, and g is the local gravity acceleration.

The stationary condition It is assumed that it can be considered as the stationary mode before the UAV takes-off, the three-axis acceleration values are only affected by the local gravity at this time. And the range of three-axis values are as shown in Figure.2(This paper uses the MPU6050 that is low-cost MEMS IMU, which has the large sensor noise).

$$\alpha \leq \sqrt{r_{ax}^2 + r_{ay}^2 + r_{az}^2} \tag{27}$$

Where $[r_{ax}^2, r_{ay}^2, r_{az}^2]^T$ is the measurement noise variance of acceleration which can be setted in the initial time.

$$\boldsymbol{R}_a = \begin{bmatrix} r_{ax}^2 & 0 & 0 \\ 0 & r_{ay}^2 & 0 \\ 0 & 0 & r_{az}^2 \end{bmatrix} \tag{28}$$

The low-dynaminc condition When the UAV is flying, the three-axis values of acceleration has small change and can be treated as th low-dynamic condition as shown in Figure.6, and be affected by the UAV body vibration. Finally, the harmful acceleration(centripetal acceleration) can contaminate the three-axis values and result in the incorrect solution about the roll and pitch.

$$\sqrt{r_{ax}^2 + r_{ay}^2 + r_{az}^2} < \alpha \leq Threshold_a \tag{29}$$

If the α satisfis the Equation(29), and the $Threshold_a$ is setted by the experimental test. It can be tuned intelligently the R_a by the Equation(30).

$$\boldsymbol{R}_a = \frac{\alpha Threshold_a}{\sqrt{r_{ax}^2 + r_{ay}^2 + r_{az}^2}} \begin{bmatrix} r_{ax}^2 & 0 & 0 \\ 0 & r_{ay}^2 & 0 \\ 0 & 0 & r_{az}^2 \end{bmatrix} \tag{30}$$

The high-dynaminc condition Unfortunately, The UAV can be disturbed by the some terrible situations which are the wind speed, airflow and bird interference during flying period. In addition, the sudden and drastic change cause the three-aixs values of accelerometer to be unusable if the a satisfies the Equation(31). Nevertheless, it can be setted the accelerometer noise at a large parameter(r_{large}) by the Equation(32) in order to eliminate the bad three-aixs values.

$$\alpha > Threshold_a \tag{31}$$

$$\boldsymbol{R}_a = \begin{bmatrix} r_{large}^2 & 0 & 0 \\ 0 & r_{large}^2 & 0 \\ 0 & 0 & r_{large}^2 \end{bmatrix} \tag{32}$$

4.2. *Heading measurement processing in the different conditions.* The heading measurement is calculated by the three-axis magnetic field values of the magnetometer, which needs to be projected from the body system to the plane system in different conditions. Moreover, the calculation of heading can be tuned depending on the several conditions of accelerometer.

The heading calculation with accelerometer If the UAV's flight phase is in the stationary or the low-dynaminc condition, the current heading is calculated by the Equation(33), which to be projected with the help of ϕ_a and θ_a from the $[a_{fx}, a_{fy}, a_{fz}]$.

$$\begin{cases} \phi_a = atan2(-a_{fx}, -a_{az}) \\ \theta_a = atan2(a_{fx}, -a_{az}) \\ heading_a = atan2(m_x cos\theta_a + m_y sin\phi_a sin\theta_a + m_z sin\theta_a cos\phi_a, \\ \qquad\qquad m_y cos\phi_a - m_z\phi_a) \end{cases} \tag{33}$$

Where the $[m_x, m_y, m_z]$ is the three-axis magnetic field values of magnetometer in the body coordinate system.

The heading calculation without accelerometer When the UAV is in the high-dynaminc condition, the current heading is calculated by the Equation(34) and not used the three-aixs values of accelerometer, which to be better projected with the help of ϕ_q and θ_q of quaternion instead of the ϕ_a and θ_a.

$$\begin{cases} \phi_q = atan2(2(q_0q_1 + q_2q_3), 1 - 2(q_1^2 + q_2^2)) \\ \theta_q = asin(2(q_0q_2 - q_1q_3)) \\ heading_q = atan2(m_x cos\theta_q + m_y sin\phi_q sin\theta_q + m_z sin\theta_q cos\phi_q, \\ \qquad\qquad m_y cos\phi_q - m_z\phi_q) \end{cases} \tag{34}$$

5. SIMULATION AND EXPERIMENTAL RESULTS ANALYSIS.

5.1. *The data acquisition.* This paper uses the experiment platform of the Figure.1 to obtain the flight sensor data which to be logged in the Pixhawk. The data of stationary and low-dynaminc condition are collected by the Multi-rotor UAV, and the data of high-dynaminc condition by the fixed-wing UAV.

Figure 1. The data acquisition platform

5.2. *The algorithm simulation.* The simulation performance of the proposed algorithm is compared with the CF and ESKF in different conditions, and taking the states estimation results of Pixhawk as the Truth. The formula of the root mean square error about the attitude is designed in order to better verify the robustness and solution accuracy of several algorithms. The attitude accuracy is quantified by the Equations(35)(36).

$$\begin{cases} RMSE_{\phi} = \sqrt{\dfrac{1}{N}\sum_{n=1}^{N}(\hat{\phi}_k^n - \phi_k^n)^2} \\ RMSE_{\theta} = \sqrt{\dfrac{1}{N}\sum_{n=1}^{N}(\hat{\theta}_k^n - \theta_k^n)^2} \\ RMSE_{\psi} = \sqrt{\dfrac{1}{N}\sum_{n=1}^{N}(\hat{\psi}_k^n - \psi_k^n)^2} \end{cases} \tag{35}$$

Where $\hat{\phi}_k^n$, $\hat{\theta}_k^n$ and $\hat{\psi}_k^n$ are the attitude to be calculated by the several algorithms,respectively, and the ϕ_k^n, θ_k^n and ψ_k^n are the Truth from the results of Pixhawk,respectively.

$$accuracy_{euler} = \frac{A_{euler} - B_{euler}}{B_{euler}} * 100\% \tag{36}$$

Where B_{euler} is the attitude solution vaules of the SVDCKF, A_{euler} is the attitude solution values of the CF or the ESKF. e.g $accuracy_{\phi} = 30\%$, A_{ϕ} is the ϕ of the CF, and B_{ϕ} is the ϕ of the SVDCKF. The $accuracy_{\phi} = 30\%$ indicates that the attitude accuracy of SVDCKF for the ϕ is higner than the CF about 30%.

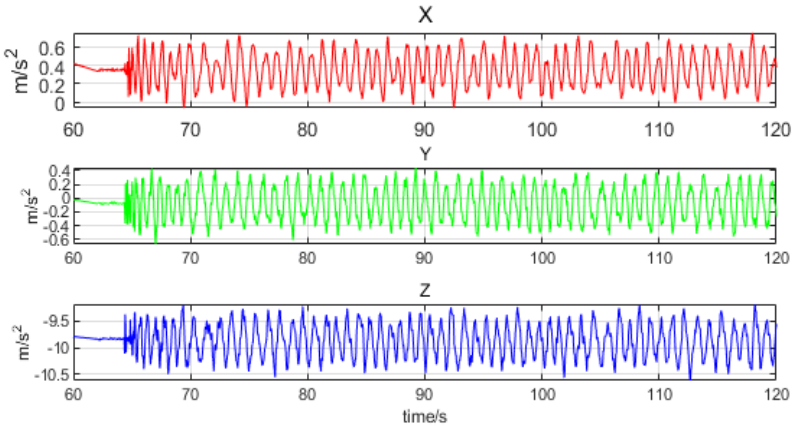

Figure 2. The values of the accelerometer in stationary condition.

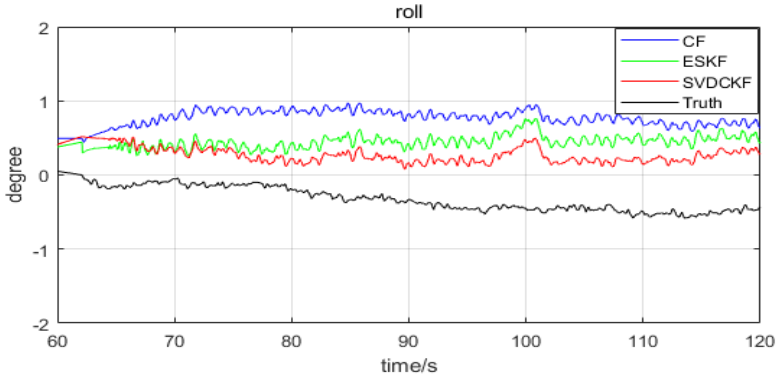

Figure 3. The roll of stationary condition.

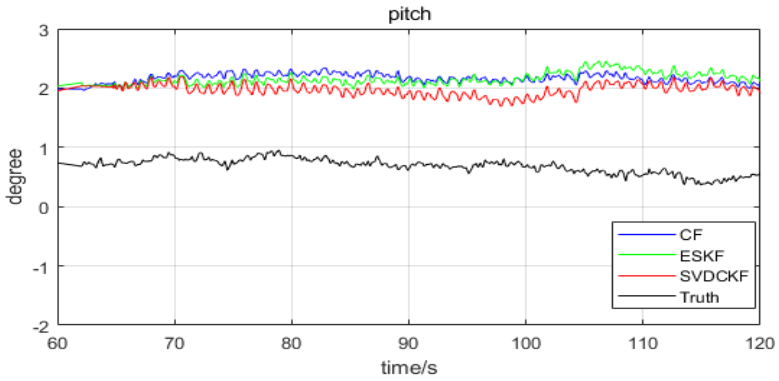

Figure 4. The pitch of stationary condition.

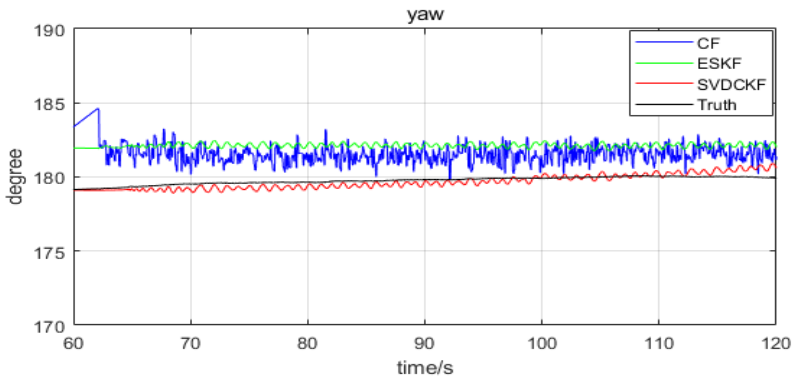

Figure 5. The yaw of stationary condition.

Table 1. Attitude RMSE(/deg) in stationary condition

Filter algorithm	CF	ESKF	SVDCKF
$RMSE_{\phi}$	1.0604	0.7334	0.5552
$RMSE_{\theta}$	1.4448	1.4061	1.2198
$RMSE_{\psi}$	1.8862	2.4380	0.2868

Table 2. The attitude accuracy(/%) in stationary condition

Accuracy	CF(SVDCKF)	ESKF(SVDCKF)
ϕ	90.9	32.1
θ	18.4	15.3
ψ	124.3	750.1

It can be seen that the range of X-axis value is the $[0, 0.6]m/s^2$, Y-axis value is the $[-0.6, 0.4]m/s^2$ and Z-axis value is the $[-10.5, -9.5]m/s^2$ in the Fig.2, respectively. Moreover, the attitude solution accuracy by the proposed algorithm is higher the both CF and ESKF in Fig.3 - 5. Nevertheless, the soultion accuracy still has certain bias compared to the Truth in the stationary condition. Why this problem happens is that this paper uses the low-cost MEMS IMU and magnetometer, which has larger sensor noises; and the states estimation results from the Pixhawk is taken as the Turth that has some errors itself. The results of Attitude RMSE(/deg) is shown in Table.1, it can be seen that the proposed algorithm has the smallest attitude root mean square error(ARMSE) in the roll, pitch and yaw, respectively. The percentage attitude accuracy of the SVDCKF compared to both CF and ESKF is listed in the Table.2.

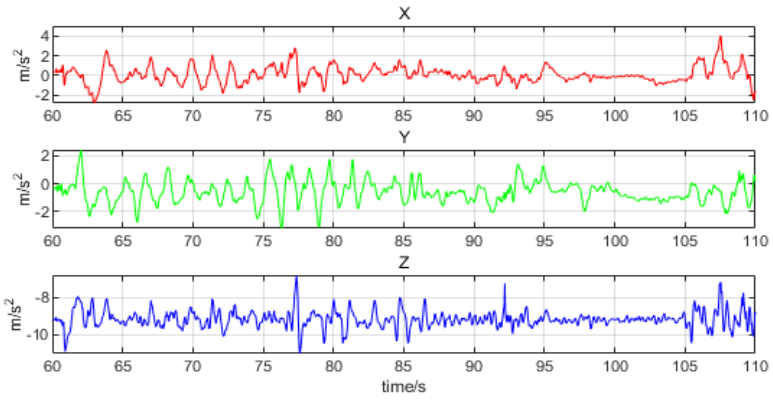

Figure 6. The values of the accelerometer during the low-dynamic condition.

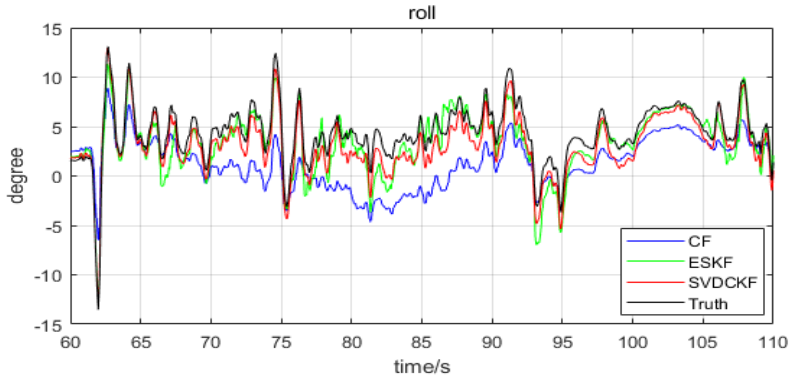

Figure 7. The roll of the low-dynamic condition.

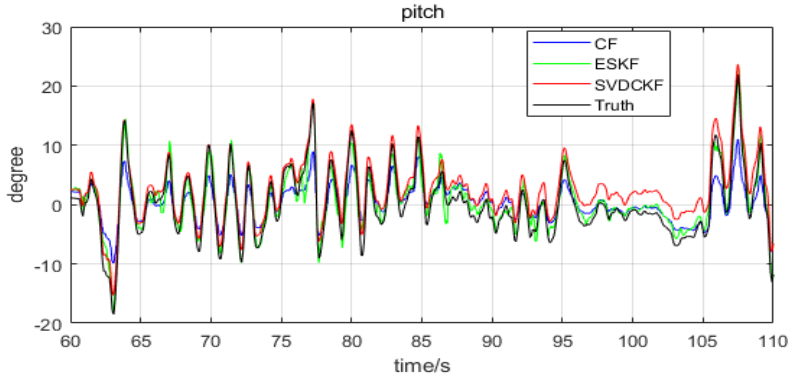

Figure 8. The pitch of the low-dynamic condition.

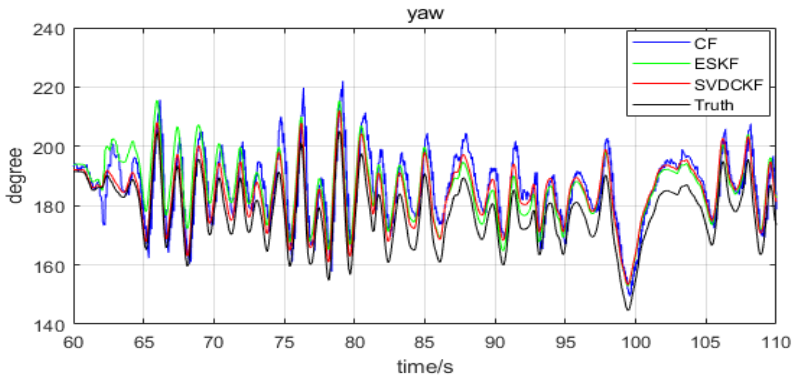

Figure 9. The yaw of the low-dynamic condition.

Table 3. Attitude RMSE(/deg) in low-dynamic condition

Filter algorithm	CF	ESKF	SVDCKF
$RMSE_\phi$	3.8586	3.7804	1.3532
$RMSE_\theta$	2.8865	3.5746	2.6406
$RMSE_\psi$	9.8283	19.3046	6.8572

Table 4. The attitude accuracy(/%) in low-dynamic condition

Accuracy	CF(SVDCKF)	ESKF(SVDCKF)
ϕ	185.1	179.4
θ	9	35.4
ψ	43.3	181.5

It can be seen that the range of X-axis value is the $[-2, 4]m/s^2$, Y-axis value is the $[-2, 2]m/s^2$ and Z-axis value is the $[-10.5, -8.5]m/s^2$ in the Fig.6, respectively. At this time, the accelerometer is disturbed by the harmful acceleration. However, the attitude solution curves of the proposed algorithm can better follow the Truth than both CF and ESKF in the Fig.7 - 9, and the results of ARMSE(/deg) is shown in Table.3. The percentage attitude accuracy of the SVDCKF compared to both CF and ESKF is listed in the Table.4.

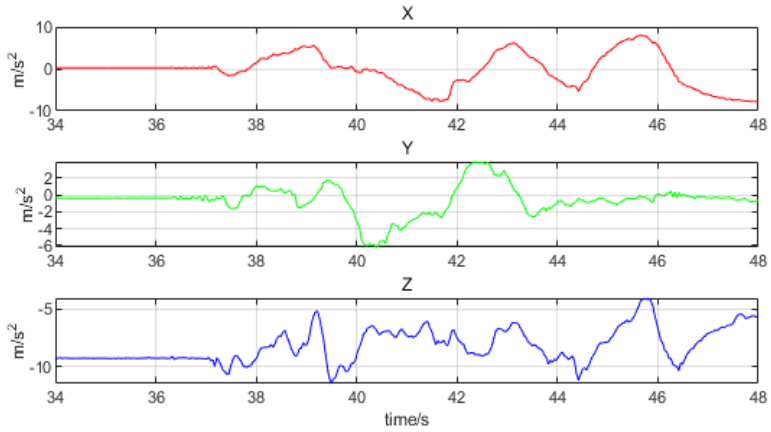

Figure 10. The values of the accelerometer during the high-dynamic condition.

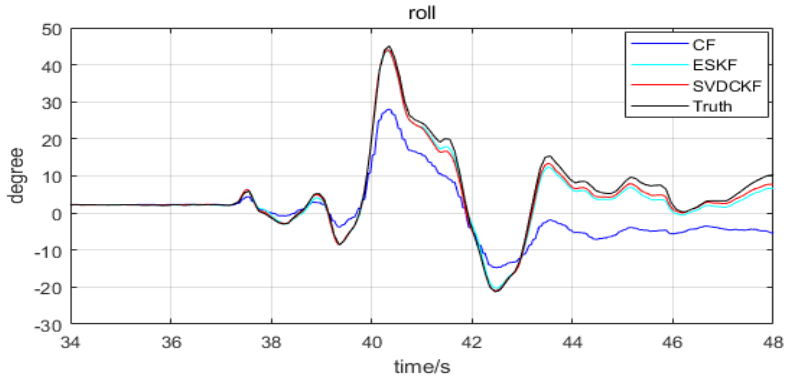

Figure 11. The roll of the high-dynamic condition.

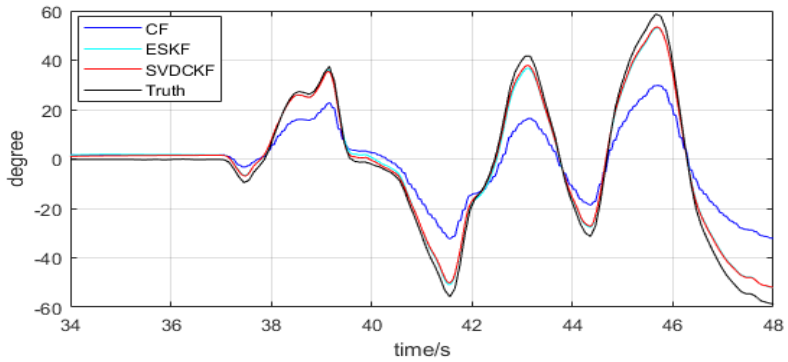

Figure 12. The pitch of the high-dynamic condition.

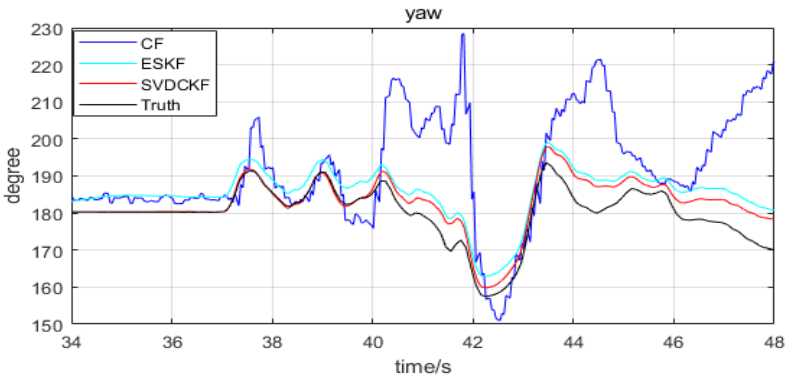

Figure 13. The yaw of the high-dynamic condition.

Table 5. Attitude RMSE(/deg) in high-dynamic condition

Filter algorithm	CF	ESKF	SVDCKF
$RMSE_\phi$	9.0373	1.7868	1.3351
$RMSE_\theta$	14.8012	3.6086	3.4363
$RMSE_\psi$	22.6943	6.2639	4.1362

Table 6. The attitude accuracy(/%) in high-dynamic condition

Accuracy	CF(SVDCKF)	ESKF(SVDCKF)
ϕ	576.9	33.8
θ	330.7	5.0
ψ	448.7	51.4

It can be seen that the range of X-axis value is the $[-10, 10]m/s^2$, Y-axis value is the $[-6, 1]m/s^2$ and Z-axis value is the $[-10.5, -4.5]m/s^2$ in the Fig.10. And it also can be shown that the high-dynamic condition is happened during the time $40s \sim 46s$ in the Fig.11 - 13, which results in the divergence of yaw solution of CF algorithm. The solution curves of the ESKF and SVDCKF can be followed with the Turth, but the solution accuracy and robustness of ESKF is not as good as the SVDCKF, and the results of ARMSE(/deg) is shown in Table.5. The percentage attitude accuracy of the SVDCKF compared to both CF and ESKF is listed in the Table.6.

6. CONCLUSION. An approach of an intelligent quaternion SVDCKF AHRS estimation with variable adaptive methods in complex conditions is proposed in this paper for the accurate attitude estimation of the small-UAV. The contributions of this paper mainly are that: (1). the nonlinear quaternion AHRS model and the sensor model are established; (2). The SVDCKF is designed to enhance the filter solution accuracy and solve the non-positive definite of the state covariance matrix P; (3). The variable adaptive methods is designed to obtain the more reliable attitude determination in different dynamic conditions of the accelerometer and magnetometer. Simulation and experimental results demonstrate that the proposed AHRS filter algorithm can effectively provide the better attitude estimation than CF and ESKF, and meets the flying requirements of the small-UAV.

Acknowledgment This paper was funded by the National Natural Science Foundation of China(grant number 6157328 61374032), This work was supported by Shaanxi Provincial Key Laboratory of Flight Control and Simulation Technology.

REFERENCES

McNeal, G. S. (2014). Drones and aerial surveillance: Considerations for legislators. Brookings Institution: The Robots Are Coming: The Project on Civilian Robotics.

Verhoeven, G. (2011). Taking computer vision aloftâĂŞarchaeological threeâĂŘdimensional reconstructions from aerial photographs with photoscan. Archaeological prospection, 18(1), 67-73.

Karaca, Y., Cicek, M., Tatli, O., Sahin, A., Pasli, S., Beser, M. F., and Turedi, S. (2018). The potential use of unmanned aircraft systems (drones) in mountain search and rescue operations. The American journal of emergency medicine, 36(4), 583-588.

Euston, M., Coote, P., Mahony, R., Kim, J., and Hamel, T. (2008, September). A complementary filter for attitude estimation of a fixed-wing UAV. In 2008 IEEE/RSJ International Conference on Intelligent Robots and Systems (pp. 340-345). IEEE.

Wu, J., Zhou, Z., Chen, J., Fourati, H., and Li, R. (2016). Fast complementary filter for attitude estimation using low-cost MARG sensors. IEEE Sensors Journal, 16(18), 6997-7007.

Yang, Q. Q., Sun, L. L., and Yang, L. (2018). A fast adaptive-gain complementary filter algorithm for attitude estimation of an unmanned aerial vehicle. The Journal of Navigation, 71(6), 1478-1491.

Madgwick, S. O., Harrison, A. J., and Vaidyanathan, R. (2011, June). Estimation of IMU and MARG orientation using a gradient descent algorithm. In 2011 IEEE international conference on rehabilitation robotics (pp. 1-7). IEEE.

Welch, G., and Bishop, G. (1995). An introduction to the Kalman filter.

Meinhold, R. J., and Singpurwalla, N. D. (1983). Understanding the Kalman filter. The American Statistician, 37(2), 123-127.

Burgers, G., Jan van Leeuwen, P., and Evensen, G. (1998). Analysis scheme in the ensemble Kalman filter. Monthly weather review, 126(6), 1719-1724.

Wang, X. X., Pan, Q., Huang, H., and Gao, A. (2012). Overview of deterministic sampling filtering algorithms for nonlinear system. Control and Decision, 27(6), 801-812.

Song, Y., Weng, X., and Guo, X. (2015). Small UAV Attitude Estimation Based on the Algorithm of Quaternion Extended Kalman Filter. Journal of Jilin University (Science Edition), 53(3).

YongLiang, W., TianMiao, W., JianHong, L., ChaoLei, W., and Chen, Z. (2008, September). Attitude estimation for small helicopter using extended kalman filter. In 2008 IEEE Conference on Robotics, Automation and Mechatronics (pp. 577-581). IEEE.

Wan, E. A., and Van Der Merwe, R. (2000, October). The unscented Kalman filter for nonlinear estimation. In Proceedings of the IEEE 2000 Adaptive Systems for Signal Processing, Communications, and Control Symposium (Cat. No. 00EX373) (pp. 153-158). Ieee.

Arulampalam, M. S., Maskell, S., Gordon, N., and Clapp, T. (2002). A tutorial on particle filters for online nonlinear/non-Gaussian Bayesian tracking. IEEE Transactions on signal processing, 50(2), 174-188.

ZHAO, L., WANG, X. X., DING, J. C., and Cao, W. (2009). Overview of nonlinear filter methods applied in integrated navigation system [J]. Journal of Chinese Inertial Technology, 1.

Pourtakdoust, S. H., and Ghanbarpour Asl, H. (2007). An adaptive unscented Kalman filter for quaternion-based orientation estimation in low-cost AHRS. Aircraft Engineering and Aerospace Technology, 79(5), 485-493.

Choukroun, D., Bar-Itzhack, I. Y., and Oshman, Y. (2006). Novel quaternion Kalman filter. IEEE Transactions on Aerospace and Electronic Systems, 42(1), 174-190.

Zhang, X., Bai, Y., Xu, Z., and Wang, R. (2015). Attitude Estimation of the Multi-rotor UAV Based on Simplified Adaptive Kalman Filter Algorithm. In Proceedings of the 2015 Chinese Intelligent Automation Conference (pp. 219-227). Springer, Berlin, Heidelberg.

Zhang, F. (1997). Quaternions and matrices of quaternions. Linear algebra and its applications, 251, 21-57.

Allan, D. W. (1966). Statistics of atomic frequency standards. Proceedings of the IEEE, 54(2), 221-230.

Allotta, B., Costanzi, R., and Fanelli, F. (2016). An attitude estimation algorithm for underwater mobile robots. IEEE/ASME Trans. Mechatronics, 21(4), 1900-1911.

Roetenberg, D., Luinge, H. J., Baten, C. T., and Veltink, P. H. (2005). Compensation of magnetic disturbances improves inertial and magnetic sensing of human body segment orientation. IEEE Transactions on neural systems and rehabilitation engineering, 13(3), 395-405.

Arasaratnam, I., and Haykin, S. (2009). Cubature kalman filters. IEEE Transactions on automatic control, 54(6), 1254-1269.

Cui, X., Jing, Z., Luo, M., Guo, Y., and Qiao, H. (2018). A new method for state of charge estimation of lithium-ion batteries using square root cubature Kalman filter. Energies, 11(1), 209.

Zhang, Q., Meng, X., Zhang, S., and Wang, Y. (2015). Singular value decomposition-based robust cubature Kalman filtering for an integrated GPS/SINS navigation system. The Journal of Navigation, 68(3), 549-562.

Wang, M., Yang, Y., Hatch, R. R., and Zhang, Y. (2004, April). Adaptive filter for a miniature MEMS based attitude and heading reference system. In PLANS 2004. Position Location and Navigation Symposium (IEEE Cat. No. 04CH37556) (pp. 193-200). IEEE.

Li, W., and Wang, J. (2013). Effective adaptive Kalman filter for MEMS-IMU/magnetometers integrated attitude and heading reference systems. The Journal of Navigation, 66(1), 99-113.